

SOFTWARE IMPLEMENTATION OF A WIDEBAND HF CHANNEL TRANSFER FUNCTION

David A. Sutherland Jr.*

This report presents an analytic model implemented as the computer program of the transfer function of a wideband HF channel model for use in a hardware simulator. The transfer function is the basic input to the hardware simulator. The mathematical basis of the program and the propagation model is presented. Parameters that characterize the skywave paths of a particular HF ionospheric condition are inputs to the program. The program code is listed and documentation is provided. Graphical verification using spectrally averaged scattering functions indicates that the transfer function program performs well and should find use as both an engineering tool and as the basis for a new standard propagation model.

Key words: channel transfer function; HF channel model; HF propagation; scattering function; wideband HF

1. INTRODUCTION

Research for and development of a wideband high-frequency (HF) radio channel simulator in hardware has been in progress for several years at the Institute for Telecommunication Sciences (ITS), see, for example, Hoffmeyer and Nesenbergs [1], Vogler et al. [2], and Vogler and Hoffmeyer [3-5]. The need for such a simulator has been driven by the renewed interest in the HF band. In particular, the HF radio band is the primary band for emergency backup communications by both amateur radio operators and Government radio systems. Thus, the HF band is important to National Security or Emergency Preparedness (NS/EP) telecommunications systems.

The HF band is characterized by widely variable conditions depending on variations in long-term solar effects (the sunspot cycle) on the ionosphere, diurnal variations in the skywave channel, fading characteristics, man-made (ignition) and natural (lightning) noise, and interference due to the crowded worldwide spectrum. These variable characteristics of the channels in the HF band make it desirable to test radio systems and subsystems in the laboratory rather than incur the costs and complexity of actual point-to-point and network tests. For example, low-power spread spectrum and frequency-hopping systems may be effective in mitigating the harsh HF environment. Wideband simulation may be useful in testing the effectiveness of these systems in the laboratory, see, for example, Redding and Weddle [6]. Narrowband simulation, since it is usually limited to less than 12 kHz, is clearly insufficient in this regard.

* The author is with the Institute for Telecommunication Sciences, National Telecommunications and Information Administration, U.S. Department of Commerce, 325 Broadway, Boulder, CO 80303.

Unfortunately, HF channel simulation has mostly depended on narrowband simulators. The most widely recognized narrowband model is the Watterson model given in Watterson, Juroshek, and Bensema [7]. The Watterson model, although widely used, is extremely restricted, as Watterson himself made quite clear. The limitations include bandwidths less than 12 kHz, negligible delay dispersion, and a single skywave path. The Watterson model is also limited to channels with stationary behavior in delay and in frequency. As a result, hardware simulators depending on the Watterson model are valid only for bandwidth-limited, stable, and stationary channels. Hence, there is an ongoing need for a much wider bandwidth simulation model that more closely models the ionospheric effects of dispersion and multipath seen over HF channels. This is even more important now that digital signal-processing (DSP) technology is being developed and improved to handle the extreme effects seen over an HF channel.

This report describes an analytic model, implemented in a computer program, that supports such a desired wideband HF channel simulator with a 1-MHz bandwidth. The HF channel simulator in hardware emulates several aspects of an HF time-varying channel: Doppler shift, Doppler spread, delay spread, and delay offset. Future versions of the wideband simulator will also include noise and interference effects based on the models described in Lemmon and Behm [8,9].

The C language program runs on a personal computer (PC) in either the Windows 3.1 or the Windows 95 operating systems. It implements the discrete transfer function of the HF channel in question. The discrete transfer function is the basic input for the hardware simulator. Input for the program are the parameters that characterize each of the skywave paths of the HF channel being modeled plus additional parameters that specify numerical conditions for the computing run. The output consists of two ASCII files. The first is a listing of all the input parameters and all the computing parameters used by the program. The second output file is the transfer function. It consists of the complex Fourier coefficients that characterize the transfer function at each sampling point in time.

This report is divided into two parts. Part I (consisting of Sections 2 - 4) contains background information for the channel model and information on the transfer function. Section 2 is a description of the HF channel model. Section 3 provides the mathematical basis for the calculation of the transfer function. Section 4 presents graphical verification of the software by means of scattering functions.

Part II (consisting of Sections 5 - 7) contains the program listing and the documentation. Section 5 discusses and explains specific aspects of the program such as special techniques and random number generation. Section 6 is a user's guide that explains details of the input and output files and tells how to run the program. Section 7 contains the program documentation and the program code.

Summary and reference sections follow. An appendix with the code listing of the program used to produce the data for the scattering functions of Section 4 is also included.

PART I. TECHNICAL AND BACKGROUND INFORMATION

2. THE PROPAGATION MODEL

This wideband HF channel model is given as the impulse response function

$$h(t, \tau) = \sum_{n=1}^N h_n(t, \tau), \quad (1)$$

where the independent variables are time t and delay τ , and $h_n(t, \tau)$ is the impulse response for one of N different ionospheric propagation paths (reflecting ionospheric layers) indexed by n . For each path n ,

$$h_n(t, \tau) = \sqrt{P_n(\tau)} D_n(t, \tau) \Psi_n(t, \tau), \quad (2)$$

where $P_n(\tau)$ is the delay power profile, $D_n(t, \tau)$ is the deterministic phase function, and $\Psi_n(t, \tau)$ is a stochastic modulating function.

For the n th propagation path, the delay power profile is given by

$$P_n(\tau) = A \frac{\alpha^{\alpha+1}}{\Delta \Gamma(\alpha+1)} x^\alpha e^{-\alpha x}, \quad (3)$$

where

$$x = \frac{\tau - \tau_c}{\Delta} + 1, \quad (4)$$

A is the maximum received power, α is the shape parameter, τ_c is the mean delay at the center frequency (which fixes the delay offset), $\Delta = \tau_c - \tau_l$ (which serves as a scale parameter), τ_l is the point in delay such that, for (3), $P_n(\tau_l) = 0$, and $\Gamma(\cdot)$ is the gamma function defined as

$$\Gamma(y) = \int_{s=0}^{\infty} s^{y-1} e^{-s} ds, \quad (5)$$

for y a positive integer. Equation 3 describes a form of the gamma probability distribution function. See Law and Kelton [10, p. 332] for details on the gamma distribution. An example delay power profile is shown in Figure 1 where A_{fl} is the receiver threshold, σ_τ is the delay spread at A_{fl} , and σ_c is the rise time to τ_c relative to A_{fl} with the restriction that

$$\sigma_c < \frac{\sigma_\tau}{2}. \quad (6)$$

The restriction is necessary for the existence of τ_l .

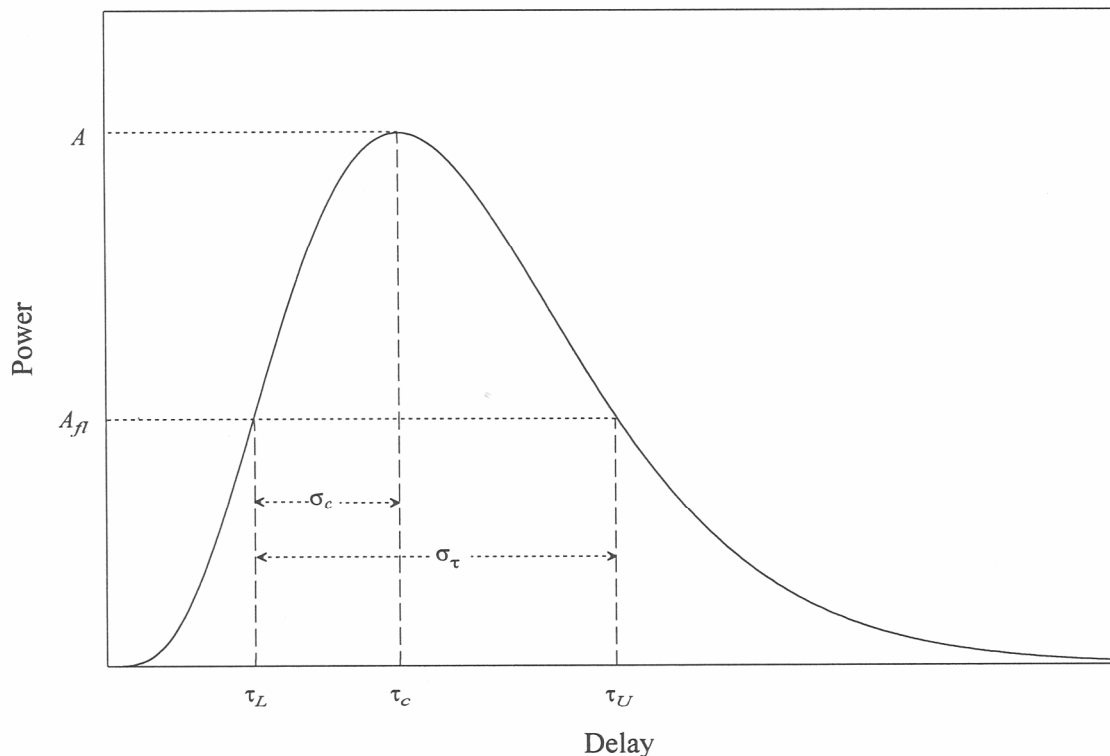


Figure 1. Delay power profile.

The deterministic phase function is given by

$$D_n(t, \tau) = \exp\{i2\pi[f_s + b(\tau - \tau_c)]t\}, \quad (7)$$

where f_s is the Doppler shift at τ_c and b is the slope or rate of change of Doppler shift with respect to τ . The dependence of phase on delay is the “slant” phenomenon described in the literature, see, for example, Wagner et al. [11].

The stochastic modulating function $\Psi_n(t, \tau)$ is a set of random processes that models the effects of the constantly changing electron density in the ionospheric-reflecting layers that cause random variations in the received signals over HF channels. In this model, the processes will exhibit exponential autocorrelation in time as well as Rayleigh fading, a widely accepted characteristic of HF propagation, see Davies [12, pp. 242-245]. The random processes used in this model are described more completely in the next section.

The channel-scattering function relates the delay spread, the delay offset, the Doppler shift, and the Doppler frequency spread. It also provides a graphical method to display the signal energy distribution. The delay spread characterizes the phase variation of a received signal, while the Doppler shift and the Doppler spread characterize frequency variation. The scattering function $S(\tau, f_D)$ is the Fourier transform of the autocorrelation function of the impulse response given by

$$S(\tau, f_D) = \int_{\Delta t = -\infty}^{\infty} R(\tau, \Delta t) e^{-i2\pi f_D \Delta t} d\Delta t, \quad (8)$$

where f_D is the Doppler frequency, Δt is the autocorrelation time lag, and $R(\tau, \Delta t)$ is the autocorrelation function of the impulse response given by

$$R(\tau, \Delta t) = C_0 \int_{t = -\infty}^{\infty} h^*(\tau, t) h(\tau, t + \Delta t) dt \quad (9)$$

where C_0 is a normalizing constant and * denotes complex conjugation, see Proakis [13, pp. 461-463]. For the Doppler spread having an exponential shape,

$$S(\tau, f_D) = P(\tau) \frac{\sigma_f}{\sigma_f + i2\pi(f_D - f_B)} e^{i2\pi\phi_0}, \quad (10)$$

where

$$f_B = f_s + b(\tau - \tau_c), \quad (11)$$

ϕ_0 is a phase term, and σ_f is a function of the Doppler spread half-width σ_D given by

$$\sigma_f = \frac{2\pi\sigma_D s_v}{\sqrt{1 - s_v^2}}, \quad (12)$$

and where

$$s_v = \frac{A_f}{A}. \quad (13)$$

More detailed explanations and descriptions of the model are given in Mastrangelo et al. [14]. The set of reports by Vogler and Hoffmeyer [3-5] also describes the development of the model. The scattering function, or ambiguity function, has been used to describe random channels in sonar and radar research as well as in HF radio. See Baggeroer [15] for an example or Middleton [16] for a general treatment.

3. THE TRANSFER FUNCTION

This section describes the discrete form of the transfer function of the channel model for implementation in a computer program. For this reason, the general mathematical definitions given in the previous section are rewritten in discrete form and are written to correspond with the functions, procedures, computations, and input parameters of the program. The channel transfer function is the discrete Fourier transform of the superimposed impulse responses given by (1) of each separate path with time held fixed.

The discrete form of the impulse response in terms of time t and delay τ is given by

$$h_{k,m} = \sqrt{P_k} c_{k,m} e^{in_{k,m}}, \quad (14)$$

where the symbols and functions are explained in detail below. The independent variables delay τ and time t are indexed by the integers $k, m = 0, 1, 2, \dots$, respectively. The discrete forms are defined as $\tau_k = \tau_0 + k\Delta \tau$ and $t_m = t_0 + m\Delta t$ where $\Delta \tau$, the delay increment, and Δt , the sampling interval, are arbitrary, but dependent on the hardware simulator's update rate, memory capacity, and bandwidth limitations.

The first factor, under the radical of (14), is the discrete form of the delay power profile given by (3). Hence, P_k determines how the impulse response behaves as a function of delay τ and is given by

$$P_k = A e^{\alpha[\ln(g)+1-g]}, \quad (15)$$

where A is the power at the expected value of delay τ_c associated with the center frequency, α is the delay spread shape factor, \ln is the natural logarithm function, and g is given by

$$g = \frac{\tau_k - \tau_l}{\sigma_l} \quad (16)$$

where l is the largest k such that, for (15), $P_l = 0$, and $\sigma_l = \tau_c - \tau_l$, which is the rise time or Δ from (3) and (4). The parameters α and τ_l are functions of the received signal threshold A_{fl} , the overall delay spread σ_τ , and σ_l . The iterative method for computing α and τ_l is discussed in the program documentation on page 20. The convenient formula in (15) is derived by taking the natural logarithm of a normalized version of (3), raising the simplified expression of the normalization to the power of e , and then multiplying by A . The normalization of (3) is obtained by taking the ratio of $P_n(\tau_k)$ to $P_n(\tau_c)$.

The last two factors of (14) describe the shape of the Doppler spread. The exponential factor is the deterministic phase function mentioned in (2) and given by (7). In the argument of the exponent,

$$\eta_{k,m} = 2\pi[f_s + b(\tau_k - \tau_c)]t_m, \quad (17)$$

where f_s is the Doppler shift at τ_c , and b is the rate of change of the Doppler shift between τ_L and τ_c , or

$$b = \frac{f_s - f_{sL}}{\tau_c - \tau_L}, \quad (18)$$

where f_{sL} is the Doppler shift at the lower end of the delay spread τ_L . Equation 17 is a linear approximation to the relationship between delay and Doppler shift. The relationship is obtained from a truncated Taylor series expansion; see section 2.1.3 in Vogler and Hoffmeyer [4]. In this program, the constant part of the Taylor's expansion, $2\pi\phi_0$, given in Vogler and Hoffmeyer [5], is set to zero, i.e., $\phi_0 = 0$; however, this factor can be allowed to vary and may be used as a correction factor. This relationship is responsible for the slanted ridges seen in scattering function measurement and is often referred to as "slant."

The factor $c_{k,m}$ represents the stochastic modulating function from (2) and is used to model the variation in the received signals observed over HF channels. The generation of these sequences in k and m is accomplished by the following single-pole infinite impulse response (IIR) filtering process on the complex random sequence ρ_m

$$c_{k,m} = (1 - \lambda)\rho_m + \lambda c_{k,m-1}, \quad (19)$$

where $c_{k,-1} = 0$ for an initial condition and

$$\lambda = e^{-\Delta t \sigma_f}, \quad (20)$$

where the factor σ_f is given by (12). As a result, the $c_{k,m}$'s, with k held fixed, will have the desired exponential autocorrelation in the time direction.

The real and imaginary parts of the sequence ρ_m are independent and identically distributed (IID) Gaussian sequences with common mean 0 and common variance 1. This is equivalent to the bivariate Gaussian process of the Watterson model which accounts for long-term fading statistics following a Rayleigh distribution, see Watterson [7].

4. VERIFICATION

Program verification is accomplished by a graphical technique. The purpose of this verification is to ensure that the program's output fairly represents the expectations of the model in terms of both the input parameters and the computed parameters. The scattering function (8) relates the delay spread, the delay offset, the Doppler shift, and the Doppler spread. The scattering function is the Fourier transform of the autocorrelation function of the impulse response. The magnitude of the scattering function $|S(\tau, f_D)|$ is used as the basic graphical verification tool.

Table 1 presents the input data used to obtain scattering functions for demonstration of verification. The input parameters are the path distance D , the center frequency f_c , the penetration frequency f_p , the layer thickness σ , the height of maximum electron density h_0 , the amplitude A , the delay spread σ_τ , the part of the delay spread below the mean delay σ_c , the Doppler spread half width σ_D , the Doppler shift at the mean delay f_s , and the Doppler shift at the lower end of the delay spread f_{sL} . Delay spreads are limited to less than 800 μs since this is a practical limitation for the channel simulator in hardware. This data is from the same set as used by Vogler and Hoffmeyer [4,5] which was obtained from Wagner, Goldstein, and Meyers [17], Basler et al. [18], and Wagner and Goldstein [19]. The reader may consult these sources for descriptions of the channel and techniques used to obtain the input parameters and the measured scattering functions. True validation of the transfer function must wait for the development of the hardware HF channel simulator. The input parameters that can be verified from the contour plots of the spectral averages at the -3-dB level are the Doppler spread $2\sigma_D$, the delay spread σ_τ , the Doppler shift at the mean delay f_s , and the Doppler shift at the lower end of the delay spread f_{sL} .

Table 1. Model Input: Skywave Path Parameters

Path	D (km)	f_c (MHz)	f_p (MHz)	σ (km)	h_0 (km)	A	σ_τ (μs)	σ_c (μs)	σ_D (Hz)	f_s (Hz)	f_{sL} (Hz)
1	126.0	5.5	13.0	30.0	265.0	1.0	70.0	34.0	0.05	0.2	0.1
2	126.0	5.5	13.0	28.0	270.0	1.0	20.0	9.0	0.05	-0.1	0.0
3	126.0	5.5	13.0	28.0	271.5	1.0	30.0	14.0	0.1	0.05	-0.05
4	88.0	2.8	5.87	30.0	240.0	0.25	350.0	170.0	5.0	1.1	0.8

In addition to the input parameters, several computed parameters may also be verified: the mean delay τ_c , the slant (the ratio of the Doppler frequency to the mean delay), and the lower and upper ends of the delay spread, τ_L and τ_U respectively. The mean delay is computed from the effective reflection height and the great circle distance between transmitter and receiver. The effective reflection height is a function of the input parameters f_c , f_p , σ , and h_0 , see p. 53 in the program documentation. This calculation depends on a hyperbolic secant-squared (sech^2) model of electron

density, see Budden [20, p. 156]. The verification parameters for the paths in Table 1 that can be verified are given in Table 2.

Figures 2 - 13 contain sequential data of the averaged spectrum at particular points in delay. A surface is fitted over the data points for purposes of illustration. The contour plots are taken from the fitted surfaces. The scales in delay may seem inconsistent since the tick marks (and grid lines) in delay represent one of the data sequences. The delay value at that point in the graph is rounded from the actual value.

Table 2. Verification Parameters

Path	$2\sigma_D$ (Hz)	σ_τ (μs)	f_s (Hz)	f_{sL} (Hz)	τ_c (μs)	slant (Hz/ μs)	τ_U (μs)	τ_L (μs)
1	0.1	70.0	0.2	0.1	1,831	0.0029	1,867	1,797
2	0.1	20.0	-0.1	0.0	1,863	-0.0111	1,874	1,854
3	0.2	30.0	0.05	-0.05	1,872	0.0071	1,888	1,858
4	10.0	350.0	1.1	0.8	1,637	0.0018	1,817	1,467

The first three paths in Tables 1 and 2 are from the ordinary mode and two extraordinary modes from 1-hop F-layer returns measured over a quiet 126-km path in California in the winter, see Wagner et al. [11].

One difficulty in studying the scattering function is in the stochastic construction of the impulse response. This makes it impossible to graphically measure parameters such as Doppler spread from the scattering function graphs, even with a quiet channel, as shown in Figure 2. Above the -3.1-dB level there is little energy exhibited in the scattering function as seen in Figure 3. This is all located in the small area at approximately 0.18 Hz and 1,810 μs . The -3-dB level is where the important parameters are displayed and graphically measured. The choice of level for verification is arbitrary, but in this model the input parameters are based at the -3-dB level. For example, the Doppler spread is measured at the mean delay, which, in this case, is 1,831 μs . As can be seen, there is no spectral energy at that point.

Smoothing techniques to rectify this problem do not suffice since there is no guarantee that the smoothed spectrum obtained from one stochastically constructed impulse response is representative of the true spectrum. Another possibility is to sample for a longer duration, but this will bring computing time and memory issues into play. Therefore, a spectral averaging technique is used to obtain a useable spectrum. Figures 4 and 5 appear more reasonable for obtaining visual verification. These figures are the average of 80 “runs” or the average of 80 separately constructed scattering functions. The program for the numerical construction of the spectrally averaged scattering function

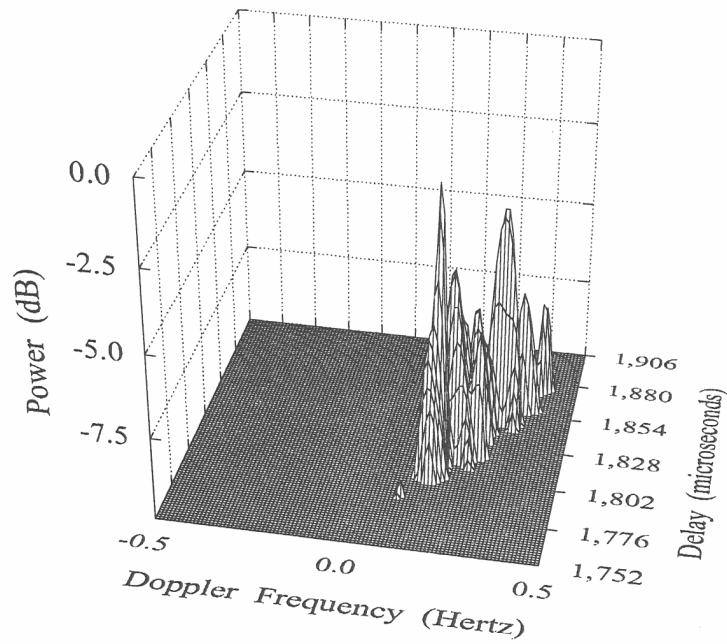


Figure 2. Scattering function above -10 dB for path 1.

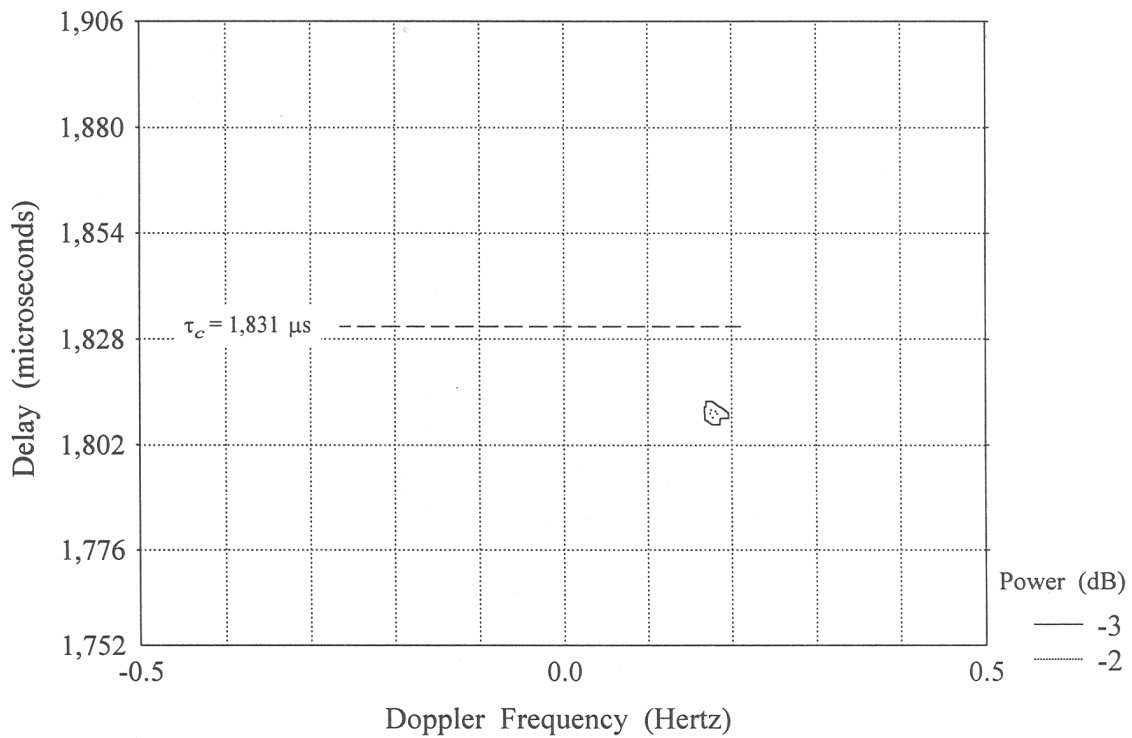


Figure 3. Scattering function contours above -3.1 dB for path 1.

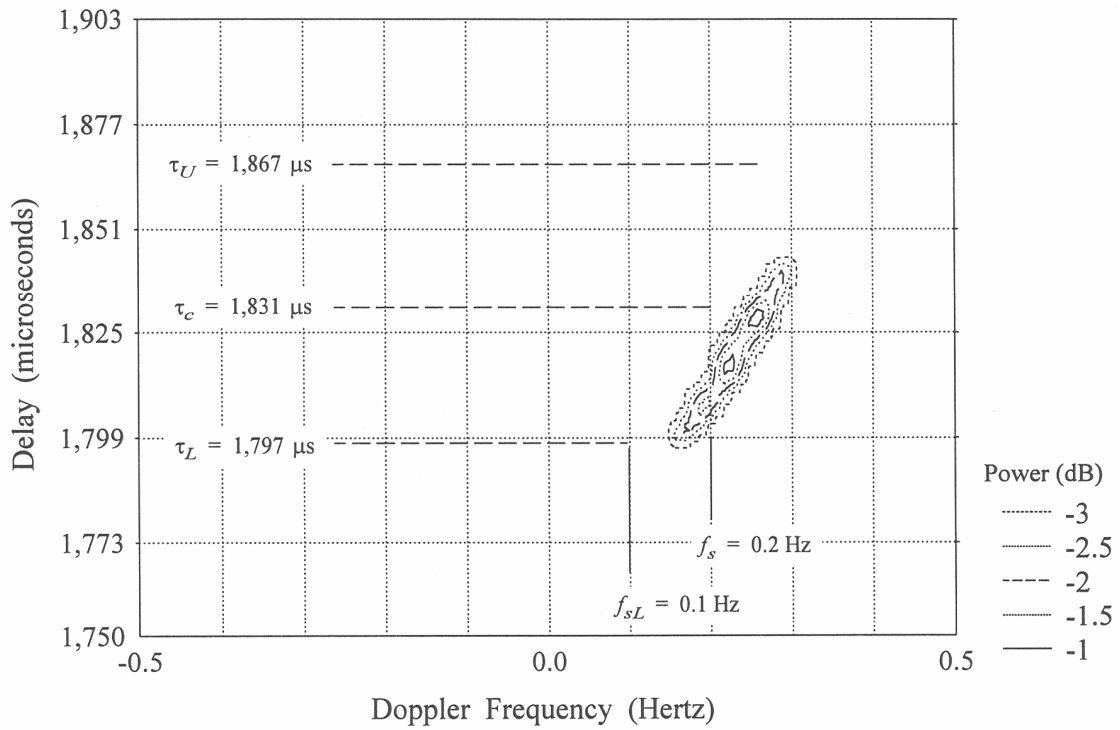


Figure 4. Spectral average contours above -3.1 dB of 80 scattering functions for path 1.

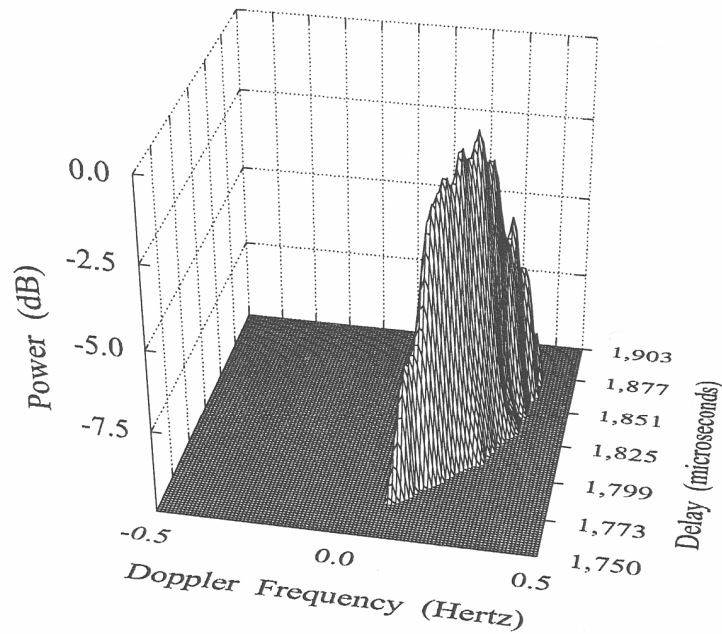


Figure 5. Spectral average above -10 dB of 80 scattering functions for path 1

is nearly identical to the transfer function program. The spectral averaging program is listed in the Appendix with documentation that describes the differences between the two programs.

The difficulty with spectral averaging is that it may take many computer runs to obtain a suitable average, especially for some ionospheric conditions, e.g., spread-F, which is defined as the phenomenon that is observed on ionograms displaying a wide range of echo pulse delay near the critical frequencies of the F layer, see, for example, Davies [12, p. 153].

Consider the first channel displayed in Figures 4 and 5. Notice that the averaged scattering function displayed in Figure 5, although considerably smoothed over that in Figure 3, still has some raggedness at the knife edge of the surface. For our purposes it still suffices for verification.

In Figure 4, the Doppler spread at the mean delay, $\tau_c = 1,831 \mu\text{s}$, measured across the -3-dB contour is approximately 0.06 Hz, which is smaller than expected by a factor of two-thirds. The delay spread across the -3-dB contour is also shorter than expected since the contours do not reach the upper end of the delay spread τ_U , although the -3-dB contour is close to the lower end of the delay spread τ_L . We estimated the slope of the line through the long axis of the -3-dB contour to be $250 \mu\text{s}/\text{Hz}$ or $0.004 \text{ Hz}/\mu\text{s}$, which is reasonably close to the predicted slant. It is believed that the discrepancies are due to the general filter design. The filter is a single pole IIR filter. Although the filter itself is a function of the sampling rate and the Doppler spread half width, it may be insufficient for accurate modeling of any one channel. Such discrepancies can be mitigated by design of digital filters to more carefully model a particular channel. This may be difficult since the raw data necessary may not be attainable due to the rapidly changing nature of the ionosphere.

The most noticeable discrepancy is that the Doppler shift at τ_c is about 0.05 Hz larger than expected. The discrepancy in Doppler shift is also noticeable at τ_L and appears to be the same offset as at τ_c . The shift appears to be constant through delay. This is also likely to be an effect caused by filtering. In this case, however, the effect may be mitigated by introducing a shift which is constant through delay. This constant shift term was mentioned in Section 3 as an arbitrary phase factor that had been set to zero. This is part of the deterministic phase function (7) which now becomes

$$D_n(t, \tau) = e^{i2\pi\{\phi_0 + [f_s + b(\tau - \tau_c)]\}}, \quad (21)$$

For path 2, there is even better graphical agreement with the parameters as seen in Figures 6 and 7. The mean delay $\tau_c = 1,863 \mu\text{s}$ appears to cut the center of the -3.0-dB contour and intersects there with the expected Doppler shift; however, the maximum indicated by the -0.5-dB contour is at $1,860 \mu\text{s}$ and -0.05 Hz . The -3.0-dB contour extends approximately $16 \mu\text{s}$, smaller than the $20\text{-}\mu\text{s}$ spread expected. The graphically measured slope of the line through the long axis of the -3.0-dB contour is $-123.81 \mu\text{s}/\text{Hz}$, which gives an estimated slant of $-0.008 \text{ Hz}/\mu\text{s}$; this is close to the expected slant of $-0.0111 \text{ Hz}/\mu\text{s}$. The Doppler spread at the mean delay is about 0.07 Hz, smaller than the 0.1-Hz spread expected at τ_c . The computed spectral average of scattering functions for this path is in fair agreement with the parameters without the discrepancies noted above for path 1.

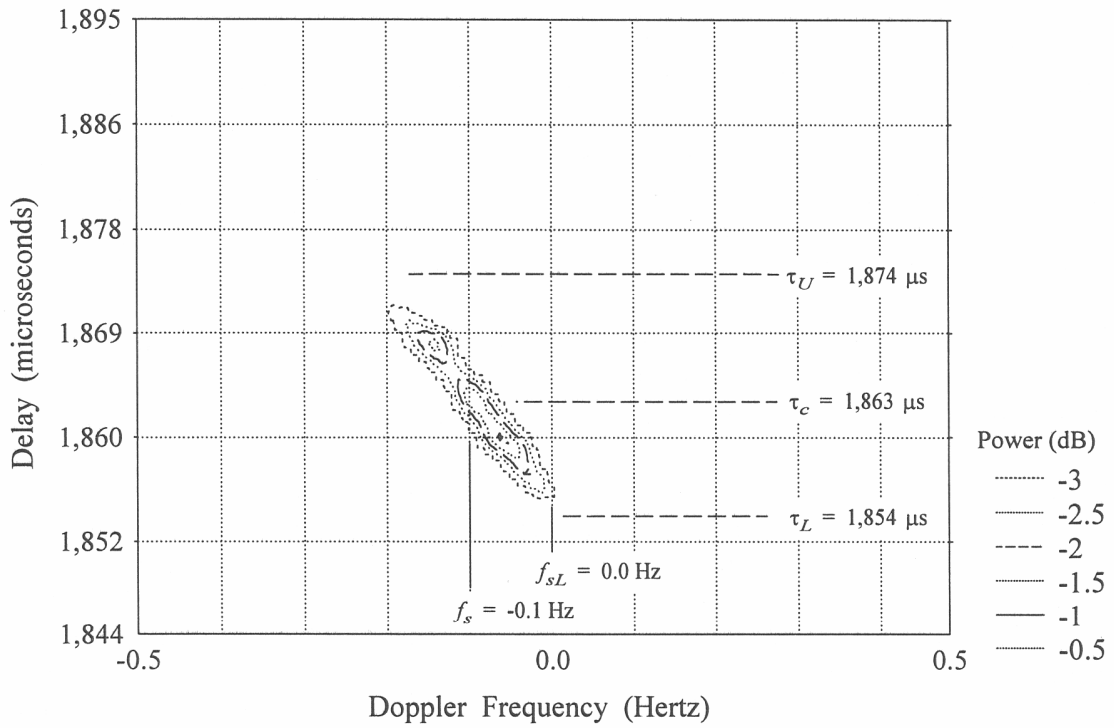


Figure 6. Spectral average contours above -3.1 dB of 80 scattering functions for path 2.

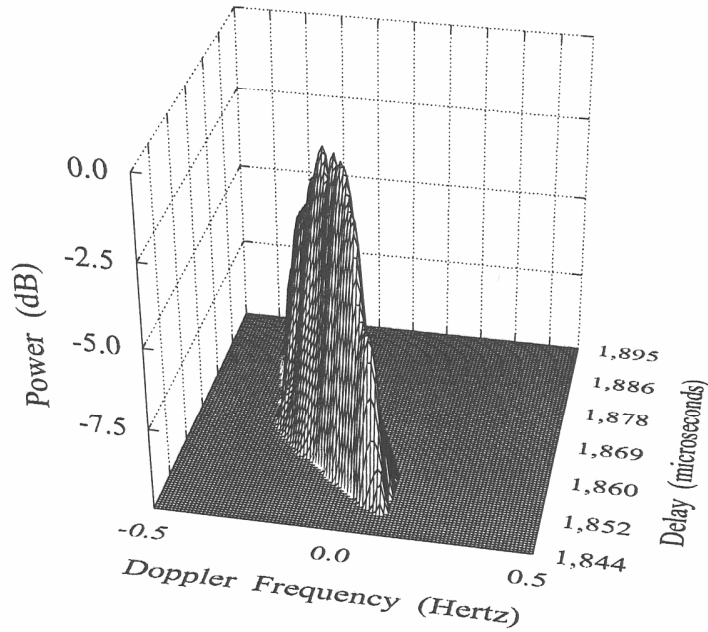


Figure 7. Spectral average above -10 dB of 80 scattering functions for path 2.

Figures 8 and 9 display the scattering function for path 3. There is a constant offset in Doppler frequency as seen before in path 1. The shift is about 0.04 Hz. The mean delay $\tau_c = 1,872 \mu\text{s}$, touches the bottom of the -1.0-dB contour. The -3.0-dB contour extends for approximately 27 μs , which is short of the 30 μs expected. The -3.0-dB level is very close to $\tau_U = 1,888 \mu\text{s}$, but $\tau_L = 1,858 \mu\text{s}$ is lower than the bottom edge of the -3.0-dB contour. Except for the shift in Doppler frequency the spectrally averaged result for this path is in fair agreement with the verification parameters.

An additional verification feature is the ability of the spectral average results to distinguish between separate paths. Figures 10 and 11 combine paths 1-3 into the actual observed situation of one ordinary mode and two extraordinary modes. Figure 10 shows two major divisions of energy. It is difficult to see the three paths on the three-dimensional rendering, but it is interesting to note that when the graphing software is “painting” the surface on the computer screen the three paths are dramatically distinct. The contour plot in Figure 11 clearly indicates the presence of three paths as the contours in the upper middle of the figure show two sections with distinctly different slopes.

Figures 12 and 13 present an intense spread-F situation over an 80-km Alaskan path, see Wagner and Goldstein [19]. The scattering function is the average of 160 runs. The mean delay of 1,637 μs appears to split the center of the contours. There is not enough resolution to clearly see the indication of slope, although the Doppler frequency at the mean delay looks reasonable; hence, there appears to be no unexpected offset in Doppler frequency as seen in two of the paths above. The Doppler spread appears to be about half of what is expected. The extent of the delay is about 65 μs short of the expected 350 μs . There appears to be good agreement with the verification parameters, but this situation probably requires more runs in order to obtain a smoother spectral average.

The model appears to agree well with the input and calculated parameters. An exception is the unexpected offset in overall Doppler frequency seen with two of the verification paths. This appears to be a function of the filter parameter λ given by (20). This parameter is itself a function of the sampling rate and the Doppler spread. This is a result of the general design of the model. The model is designed for a wide range of applications. To more carefully model a path with a particular ionospheric situation, it may be necessary to tailor the filter design to the situation. The filtering effect is also believed to be responsible for the delay shapes being shorter than expected. Another consideration is that it may be necessary to design the delay power profile (3) and (15) for the specific situation. The alternative is that the general model may need to be more complicated to fit more cases.

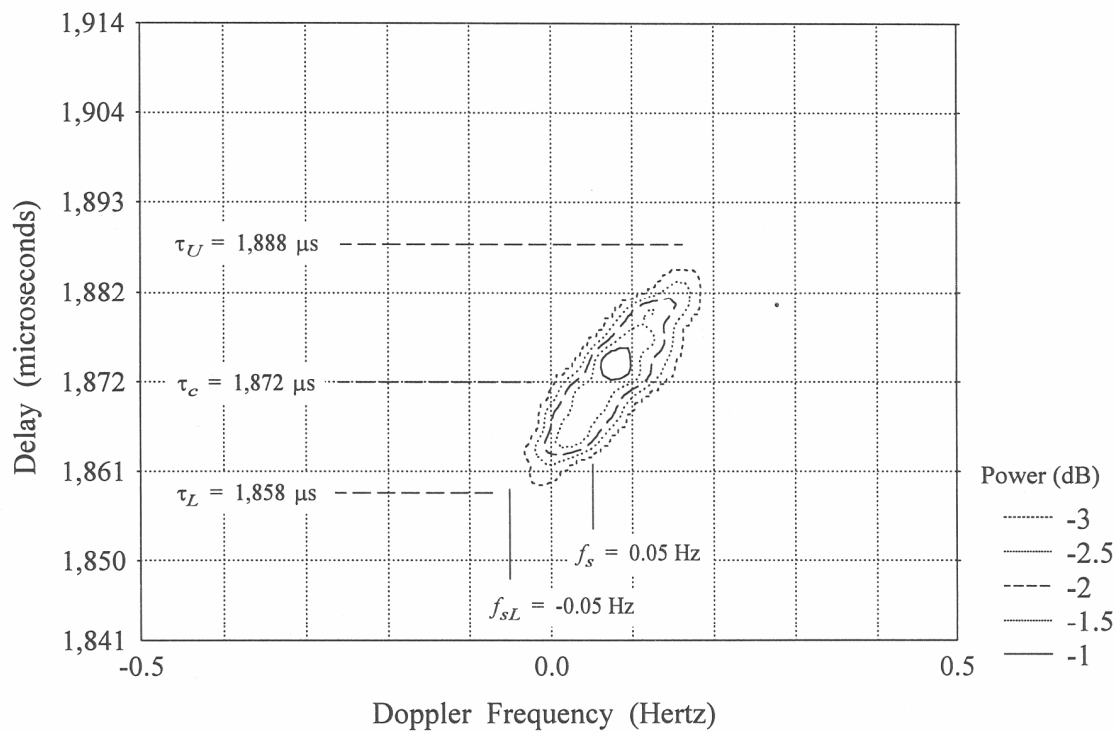


Figure 8. Spectral average contours above -3.1 dB of 80 scattering functions for path 3.

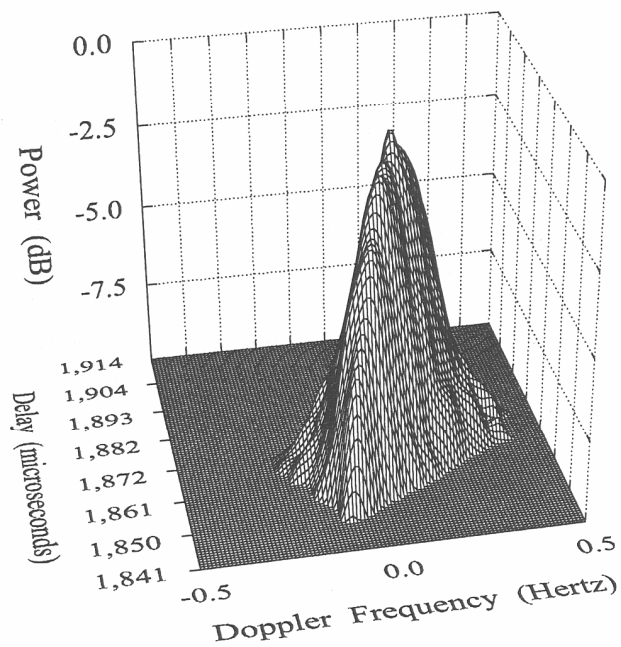


Figure 9. Spectral average above -10 dB of 80 scattering functions for path 3.

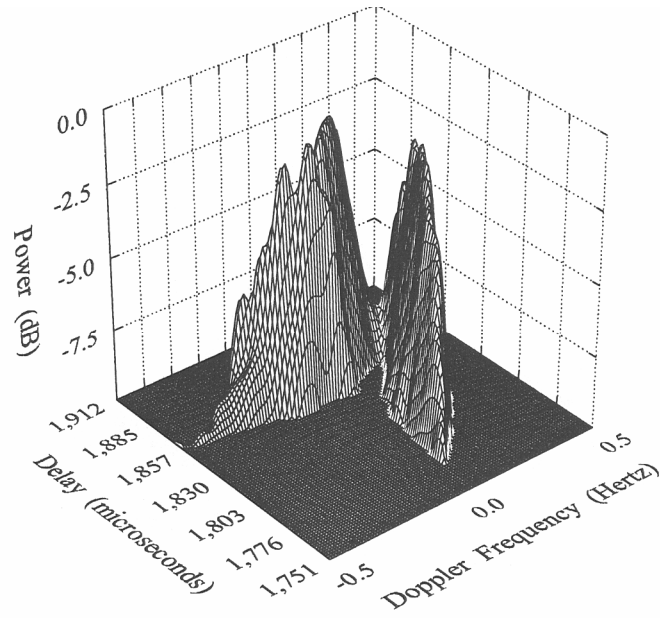


Figure 10. Spectral average above -10 dB of 80 scattering functions for paths 1, 2, and 3.

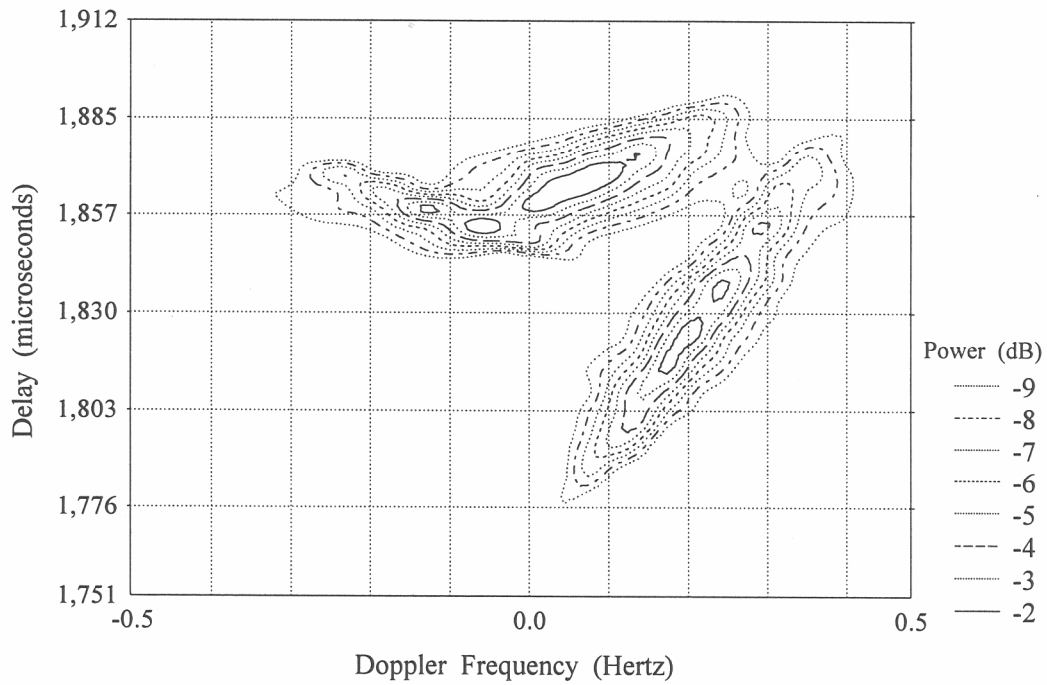


Figure 11. Spectral average contours above the -10 dB level of 80 scattering functions for paths 1, 2, and 3.

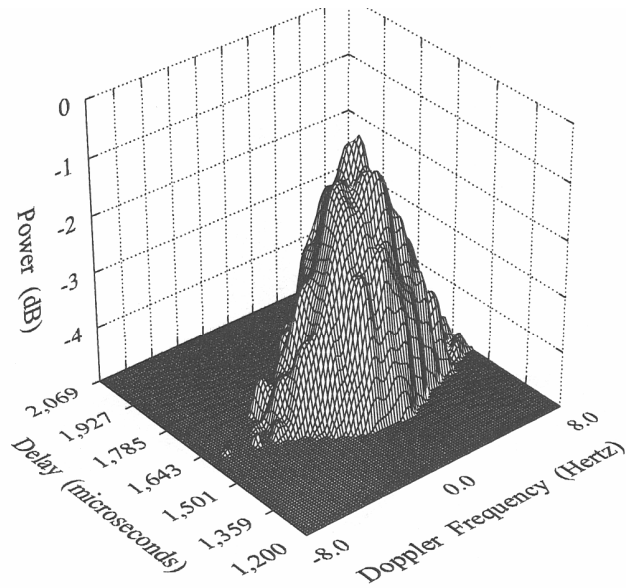


Figure 12. Spectral average above -5 dB of 160 scattering functions for path 4.

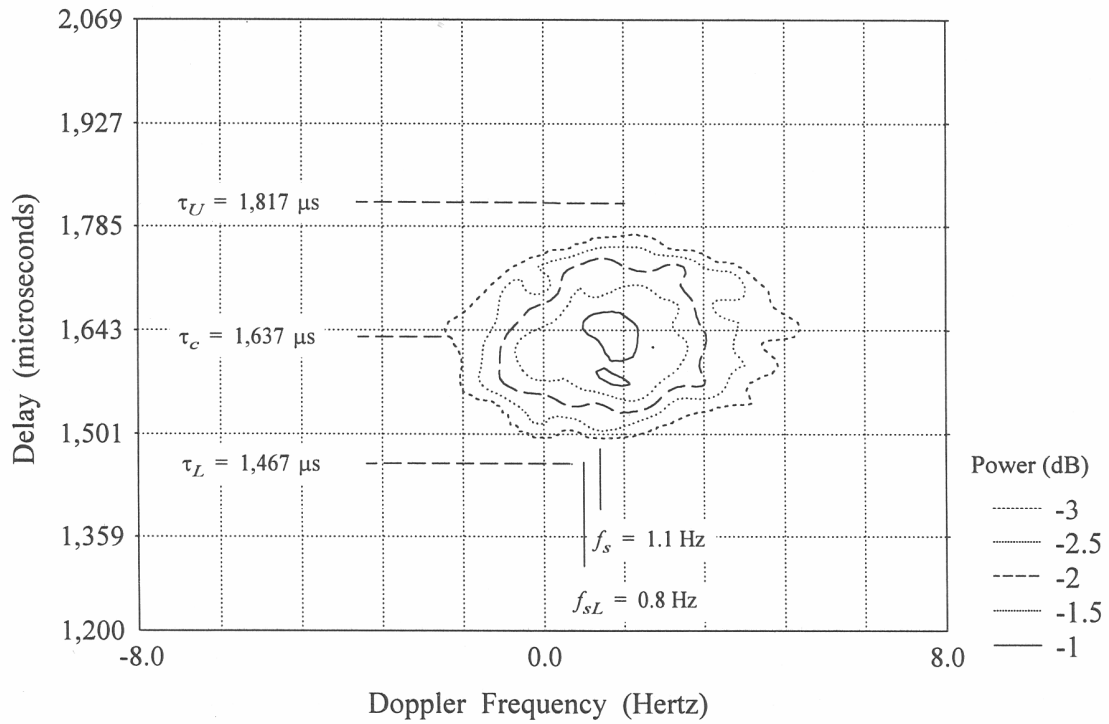


Figure 13. Spectral average contours above -3.1 dB of 160 scattering functions for path 4.